CHAPTER

# 20 Assimilation of HF Radar Observations in the Chesapeake–Delaware Bay Region Using the Navy Coastal Ocean Model (NCOM) and the Four-Dimensional Variational (4DVAR) Method

**Hans Ngodock[1,*], Philip Muscarella[1], Matthew Carrier[1], Innocent Souopgui[2], Scott Smith[1]**

*Naval Research Laboratory, Stennis Space Center, Mississippi, USA[1]; Department of Marine Science, University of Southern Mississippi, Stennis Space Center, Mississippi, USA[2]*

**Corresponding author: E-mail: hans.ngodock@nrlssc.navy.mil*

## CHAPTER OUTLINE



## 1. INTRODUCTION

Consistent and accurate coastal ocean monitoring necessitates the availability of three key components: (1) an observing network that adequately samples the monitored domain, (2) a coastal ocean circulation model with a sufficiently high

Coastal Ocean Observing Systems. http://dx.doi.org/10.1016/B978-0-12-802022-7.00020-1

resolution that takes into account the often complex geometry and dynamics that occur near the coastline, and (3) an analysis system that is able to accurately assimilate the sampled observations to initialize the coastal model for forecasting. Modern analysis systems can also provide an observation impact assessment for the design, evaluation, and possibly reassignment of observing resources.

Coastal current measurement types are limited to moored buoys and ADCPs, which do not provide adequate spatial distribution/resolution, surface drifters, which tend to leave the deployment area relatively quickly, and shipboard ADCPs, which are relatively expensive to operate. The continuous monitoring of coastal waters for circulation properties requires long-term station observations. High-frequency (HF) radar units are unique observation platforms that provide surface current measurements at horizontal resolutions of 1 to 6 km ranging from 25 to 200 km off the coast. This amount of spatial coverage would be unattainable with current meter stations. In addition, HF radar units are installed by various universities and institutions along much of the coastline of the continental United States. HF radar observations have been assimilated into ocean models mostly using sequential methods (e.g., Refs 1–4). However, there are a few assimilation examples using a 4DVAR method.[5–7]

Regional ocean models for coastal circulation monitoring require initial and boundary conditions from larger or global domain models that are usually run with much coarser horizontal resolution, as well as surface forcing fields from atmospheric models. To a large extent, the accuracy of the coastal models depends on (1) the accuracy of the larger domain model providing initial and boundary conditions, (2) the accuracy of the atmospheric model providing surface forcing fields, and equally important, (3) the accuracy of the parameterization of the physics due to increased resolution. The increased resolution can also become a liability for the assimilation as the model resolves small-scale circulation features that cannot be constrained by the available observations. Usually, only coarse observation coverage is available for assimilation into the larger domain (with the exception of sea surface temperature (SST)), making it difficult to provide accurate initial and boundary conditions for the coastal model. Also, atmospheric models can contain errors in the coastal oceans due to the coarse resolution often used and the complex land–sea boundary, not to mention the lack of frequent feedback from the ocean to the atmosphere in these areas. Failure to do this also translates to errors in the atmospheric fields in these areas. In addition, the ocean model's horizontal resolution may not be high enough to capture all the details of the coastline and the bathymetry. All these elements contribute to the discrepancies that are seen when coastal ocean model solutions are compared to observations. This is where the data assimilation plays the critical role of combining the ocean model and available observations in a dynamically consistent way to not only provide a better initial condition for the prediction of the ocean environment, but also to correct at least some components of the model error, e.g., errors in the atmospheric forcing fields.

Due to the high temporal variability of surface currents in the coastal areas, a necessary requirement of the assimilation system is the ability to take into account the temporal dimension in the observations. Such capability is inherent to 4DVAR.

Contrary to the often used sequential methods that assimilate observations at a given time (thus correcting the model state at fixed time stamps), e.g., the three-dimensional variational data assimilation (3DVAR), or the methods based on the Kalman filter, 4DVAR seeks to correct the entire model trajectory for a given time window by assimilating all the observations (distributed in time and space) that were sampled during that time window. In this process, 4DVAR (1) uses observations at almost the exact times that they are sampled, which suits most asynoptic data, (2) implicitly uses flow-dependent background errors, which ensures the analysis quality for rapidly changing environments, and (3) uses a forecast model as a constraint, which ensures the dynamic balance of the final analysis.

It was recently shown that the assimilation of surface velocity observations derived from drifters, using a 4DVAR with the Naval Coastal Ocean Model (NCOM-4DVAR[8]), improved ocean model forecasts of sea surface height, surface and subsurface velocity, temperature, and salinity in the Gulf of Mexico.[9] Unfortunately, this study was limited in time due to the deployment and lifespan of the drifters. This paper aims to expand on the previous study by assimilating a sustained and dense source of surface velocity observations from HF radars in the Chesapeake–Delaware Bay region to show that they are a viable dataset for constraining and forecasting the coastal circulation.

## 2. HF RADAR OBSERVATIONS

The surface current observations used for this study come from a network of three SeaSonde HF radar units that are deployed in the mid-Atlantic region of the East Coast of the United States (black stars on Figure 1). The northernmost site is on Assateague Island, Maryland, the central site is at Cedar Island, Virginia, and the southernmost site is at Little Island Park, Virginia. Throughout the study period, data is available from these sites during 93%, 99.9%, and 100% of the time, respectively. These HF radar units produced by CODAR ocean sensors scatter radio waves off the ocean surface and infer movement of near surface currents. During July 2013, the three stations were operating at 4.5 MHz that resonantly scatter off surface gravity waves of approximately 30-m wavelength. For these so-called long-range site observations are provided hourly on a polar-coordinate grid with a range step of 6 km and a bearing step of 5°. Additionally, the horizontal range of a single site is approximately 200 km offshore.

Roarty et al.[10] discusses the operation and maintenance of the mid-Atlantic HF radar observing network; this includes the three sites used in this study. Because the HF radar data is used by the U.S. Coast Guard Search and Rescue Optimal Planning System (SAROPS), there is an implemented procedure for quality control and assurance of the observations collected by these sites. Additionally, they go on to report RMS differences between in situ measurements of both acoustic doppler current profilers (ADCPs) and drifters of 7.4 to 9.8 cm/s using an unweighted least squares method.[11] This unweighted least squares approach merges the single-site radial

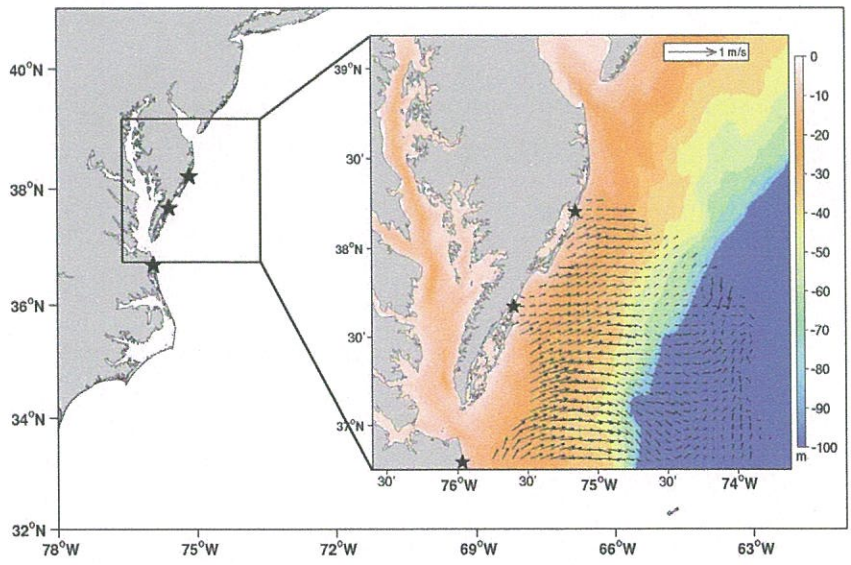


**FIGURE 1**

The model domain: the outer box is the 3-km parent nest, and the inner and expanded box is the actual 1-km domain with a sample coverage of HR radar observations on July 01, 2013, overlaid on the colored bathymetry. The radar stations are represented by the stars.

velocities located within a search radius around each grid point. This processing step uses a Matlab toolbox called HFR_Progs to create total current vectors. For the three-site setup used here, the search radius is 10 km with a minimum of two radials from at least two sites required to create a total. In theory, accurate surface velocities are recovered when two HR radar beams form an angle of 90°. In practice, however, accurate velocities can still be constructed from beams forming an angle as low as 15°, which has become a standard for operational processing of HF radar observations, at least in the mid-Atlantic Bight HF radar observing network.[10] The HF radar observations assimilated here were processed with the 15° minimum angle threshold. The HF radar measurements are sensitive to environmental factors that can affect the spatial extent of the velocity footprint. This usually results in occasional gaps within a coverage area. For more information see Ref. 12.

## 3. THE MODEL

The ocean model used in this study is the Navy coastal ocean model (NCOM). NCOM is a free-surface model that has been described in the literature.[13,14] The model domain (and bathymetry) shown in Figure 1 spans longitudes 76.6°W to 73.6°W and latitudes 36.75°N to 39.2°N at 1-km horizontal resolution with 50

vertical levels. The initial conditions were obtained from downscaling the operational 1/8° resolution global NCOM (GNCOM) to an intermediate model with horizontal resolution of 3 km, and then to a high-resolution 1-km model. Horizontal viscosities and diffusivities are computed using either the grid-cell Reynolds number (Re) or the Smagorinsky schemes, both of which tend to decrease as resolution is increased. The grid-cell Re scheme sets the mixing coefficient $K$ to maintain a grid cell Re number below a specified value, e.g., if $\mathrm{Re} = \mathrm{u} * \mathrm{dx}/K = 30$, then $K = \mathrm{u} * \mathrm{dx}/30$. Hence, as dx decreases, $K$ decreases proportionally. A similar computation is performed for the Smagorinsky scheme.

The surface atmospheric forcing, including wind stress, atmospheric pressure, and surface heat flux, is provided by the Navy Global Atmospheric Prediction System (NOGAPS[15–17]) with a horizontal resolution of 0.5°. River forcing is provided at all river in-flow locations in this mid-Atlantic domain. Additionally, eight tidal constituents (K1, O1, P1, Q1, K2, M2, N2, and S2) are forcing the domain through the open boundaries. Open boundary conditions use a combination of radiative models and prescribed values provided by the parent 3-km nest. Different radiative options are used at the open boundaries depending on the model state variables: a modified Orlanski radiative model is used for the tracer fields (temperature and salinity), an advective model for the zonal velocity (u), a zero gradient condition for the meridional velocity (v) as well as the barotropic velocities, and the Flather boundary condition for elevation.

## 4. THE ASSIMILATION SYSTEM

The assimilation system used here is described in more detail in Ref. 8. The brief presentation that follows only serves to elucidate the focus of this study. For a given model, the following is presented:

$$\begin{cases} \dfrac{\partial X}{\partial t} = F(X) + f, \; 0 \le t \le T \\ X(t=0) = I(x) + i(x) \end{cases} \tag{1}$$

where $X$ stands for all the dependent model state variables, i.e., the two-dimensional SSH and barotropic velocities, and the three-dimensional temperature, salinity, and baroclinic velocities; $F$ includes the model tendency and forcing terms, $f$ is the model error with covariance $C_f$, $I(x)$ is the prior initial condition, and $i(x)$ is the initial condition error with covariance $C_i$; $x$ and $t$ represent the position in the three-dimensional space and time, respectively. Given a vector $Y$ of $M$ observations of the model state in the space–time domain, with the associated vector of observation errors $\varepsilon$ (with covariance $C_\varepsilon$), the following is shown:

$$y_m = H_m X + \varepsilon_m, \quad 1 \le m \le M \tag{2}$$

where $H_m$ is the observation operator associated with the $m$th observation. One can define a weighted cost function as follows:

$$J = \int_0^T \int_\Omega \int_0^T \int_\Omega f(x,t) W_f(x,t,x',t') f(x',t') dx' dt' dx dt + \int_\Omega \int_\Omega i(x) W_i(x,x') i(x') dx' dx + \varepsilon^T W_\varepsilon \varepsilon \tag{3}$$

where $\Omega$ denotes the model domain, the weights $W_f$ and $W_i$ are defined as inverses of $C_f$ and $C_i$ in a convolution sense, and $W_\varepsilon$ is the matrix inverse of $C_\varepsilon$. Boundary condition errors are omitted from Eqns (1) and (3) only for the sake of clarity. The solution of the assimilation problem, i.e., the minimization of the cost function (Eqn (3)), is achieved by solving the following Euler-Lagrange (EL) system:

$$\begin{cases} \dfrac{\partial X}{\partial t} = F(X) + C_f \cdot \lambda, \ 0 \le t \le T, \\ X(t=0) = I(x) + C_i \circ \lambda(x,0) \\ -\dfrac{\partial \lambda}{\partial t} = \left[\dfrac{\partial F}{\partial X}(X)\right]^T \lambda + \sum_{m=1}^{M} \sum_{n=1}^{M} W_{\varepsilon,mn} (y_m - H_m X) \delta(x - x_m) \delta(t - t_m), \quad 0 \le t \le T \\ \lambda(T) = 0 \end{cases} \tag{4}$$

where $\lambda$ is the adjoint variable defined as the weighted residual:

$$\lambda(x,t) = \int_0^T \int_\Omega W_f(x,t,x',t') f(x',t') dx' dt', \tag{5}$$

and $\delta$ denotes the Dirac delta function, $W_{\varepsilon,mn}$ are the matrix elements of $W_\varepsilon$, the superscript $T$ denotes the transposition, and the covariance multiplication with the adjoint variable is the convolution:

$$C_f \cdot \lambda(x,t) = \int_0^T \int_\Omega C_f(x,t,x',t') \lambda(x',t') dx' dt', \tag{6}$$

and

$$C_i \circ \lambda(x,0) = \int_\Omega C_i(x,x') \lambda(x',0) dx' \tag{7}$$

for the model and initial condition errors, respectively.

It can be seen in Eqn (4) that the adjoint model is forced by the innovations (model-data misfits at the observation locations), and its solution initializes and/or forces the forward model, depending on whether a strong or weak constraints assumption is adopted.

A standard approach to solving the Euler-Lagrange system (Eqn (4)) is the strong constraints *4dvar* that assumes that only the initial condition is erroneous, i.e., the model has no errors ($C_f = 0$). The solution of Eqn (4) is found iteratively as follows: (1) a first guess initial condition is used to solve the nonlinear model, (2) the nonlinear solution is used to compute the model-data misfits that appear in the right-hand side of the adjoint model, (3) the adjoint model is solved and used to compute the correction to the initial condition, and (4) the process is repeated until the minimum of the cost function or a preselected convergence criterion is reached.

The weak constraints 4dvar approach takes into account the model errors and, thus, increases the dimension of the control space, which now becomes the entire model trajectory for the selected assimilation window. This rather huge control space also increases the computational cost of the assimilation, and it usually renders the minimization (of the cost function) process poorly conditioned. This difficulty can be avoided if the minimization is done in the data space, which does not depend on and is usually much smaller than the control space. That is possible through the representer algorithm,[18,19] which expresses the solution of Eqn (4) as the sum of a first guess and a finite linear combination of representer functions, one per datum. Being a linear expansion, the representer algorithm cannot be applied to Eqn (4) directly, mainly because of its nonlinear property. However, following Refs 8,20 the representer algorithm can be applied to a linearized form of Eqn (4).

## 5. EXPERIMENTS AND RESULTS

For this study, the initial condition error for the experiment is set as 1.0 °C for temperature, 0.1 practical salinity unit (psu) for salinity, and 0.5 m/s for velocity. These errors are set by examining the innovation values between a free-running NCOM and available observations. The error values are uniformly prescribed across the domain and reduced at depth. This is deemed acceptable because we are mostly interested in the accuracy of surface currents. It is also important to note the model errors in this study are attributed to errors in the specified atmospheric surface forcing. This a reasonable assumption as ocean surface currents are strongly influence by surface wind stress. The model errors are 0.05 °C for temperature, 0.005 practical salinity unit (psu) for salinity, and 0.05 m/s for velocity. The model errors represent 5% of the magnitudes of the atmospheric forcing in respective equations, with the exception of the free surface, and are converted from fluxes units to units of the ocean state variables using the relationships imposed by the discretization of the model (see Refs 21,8). The horizontal correlation scales of the initial and model errors are taken to be 20 km (approximately the Rossby radius of deformation

in the domain) and fixed in time. When these isotropic covariances are convolved with the adjoint solution and included in the forward model as dictated by Eqn (4), the 4dvar system produces analysis increments that are flow dependent, thanks to the dynamics of the tangent linear and adjoint models, and also the nonlinear model trajectory around which the system is linearized.

Each of the observation data types is also assigned errors. The observation errors are usually a combination of the estimated instrument error and the representativeness error. Here, the temperature error is 0.35 °C, 0.035 practical salinity unit (psu), and 0.05 m/s for velocity. The experiment carried out here takes place from July 1 to 31, 2013, in sequential assimilation windows of three days, with observations binned hourly and subsampled to keep only one observation per 20-km correlation scale in both meridional and zonal directions. With the exception of the first cycle, the background (i.e., the solution that the assimilation is trying to correct) for each cycle is the forecast obtained by running the nonlinear with the final condition from the analysis in the previous cycle.

In order to assess the fit to the observations over time in the whole assimilation window, we define the following "fit to the observations" metric:

$$J_{FIT} = \frac{1}{M} \sum_{m=1}^{M} \frac{\left| y_m - H_m X^a \right|}{\sigma_m}. \tag{8}$$

In Eqn (8), $y_m$ is the $m$th observation, $M$ is the total number of observations, $H_m$ is the observation operator, $X^a$ is the assimilated solution or analysis, and $\sigma_m$ is the observation error or standard deviation. The right-hand side of Eqn (8) can be computed as a time series and also evaluated for the free-run solution and the first guess. Because the assimilation is expected to fit the observations to within the observation standard deviation at the observation locations, the metric $J_{FIT}$ in Eqn (8) is expected to be less or equal to one for the analysis. One only hopes that the same is true for the subsequent forecasts as a result of fitting the observations in previous cycles.

The results of this assimilation experiment show that the NCOM-4DVAR is capable of assimilating HF radar velocities by significantly reducing the discrepancies between the modeled and the observed surface velocities. It can be seen in Figure 2 that the free-running model for the 1-km resolution (black line) is in significant disagreement with the observations, having $J_{FIT}$ values between 2 and 4 observation standard deviations. The assimilation (gray dashed line) is able to reduce those discrepancies, sometimes by as much as 2 standard deviations, with $J_{FIT}$ values generally between 1 and 2.4 observation standard deviations. These values are still higher than the target value of 1, indicating that, although the assimilation has done a good job of reducing the discrepancies compared to the free-running model, the assimilated solution is still not fitting the observations accurately. On the other hand, the first guess solution (dashed black line), which consists of the forecast from analysis in the previous assimilation window, shows discrepancies of the same magnitudes as the free-running solution. This indicates that the gains of the

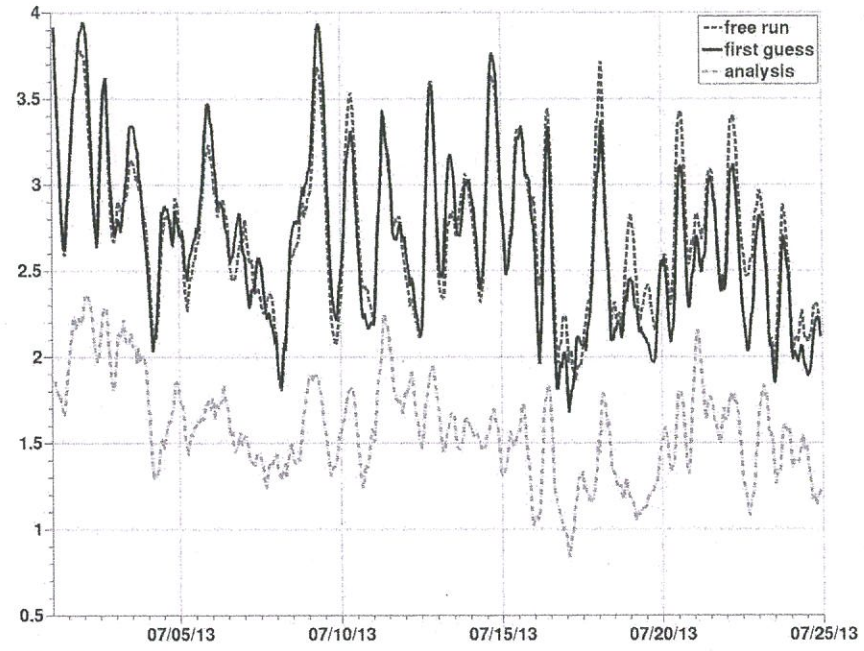


**FIGURE 2**

The $J_{FIT}$ metric for a free-running model (black dashed line), the 4DVAR first guess fields (solid black line), and the 4DVAR analysis (gray dashed line) at the observation locations. This experiment assimilates observations hourly.

assimilation are quickly lost in the forecast, primarily due to erroneous surface forcing and the high resolution of the model that resolves circulation features that are not observed.

## 6. VALIDATION

The validation of any assimilation experiment requires independent observations against which the assimilation results can be compared. Those usually consist of buoys along the coast. However, those are not available during the time of this experiment. We carried out a second assimilation experiment where observations are assimilated every 3 h instead of every hour as in the previous experiment. The unassimilated observations, i.e., those that are left out every 2 h, are considered independent for the purpose of validation, even though they may be correlated with those that are assimilated, by reason of proximity in space and time. The same fit to the observations metric $J_{FIT}$ is also used to evaluate this assimilation experiment, not only for the assimilated observations, but also for the withheld observations. Results in Figure 3(a) show the $J_{FIT}$ values for the assimilated solution and the first guess

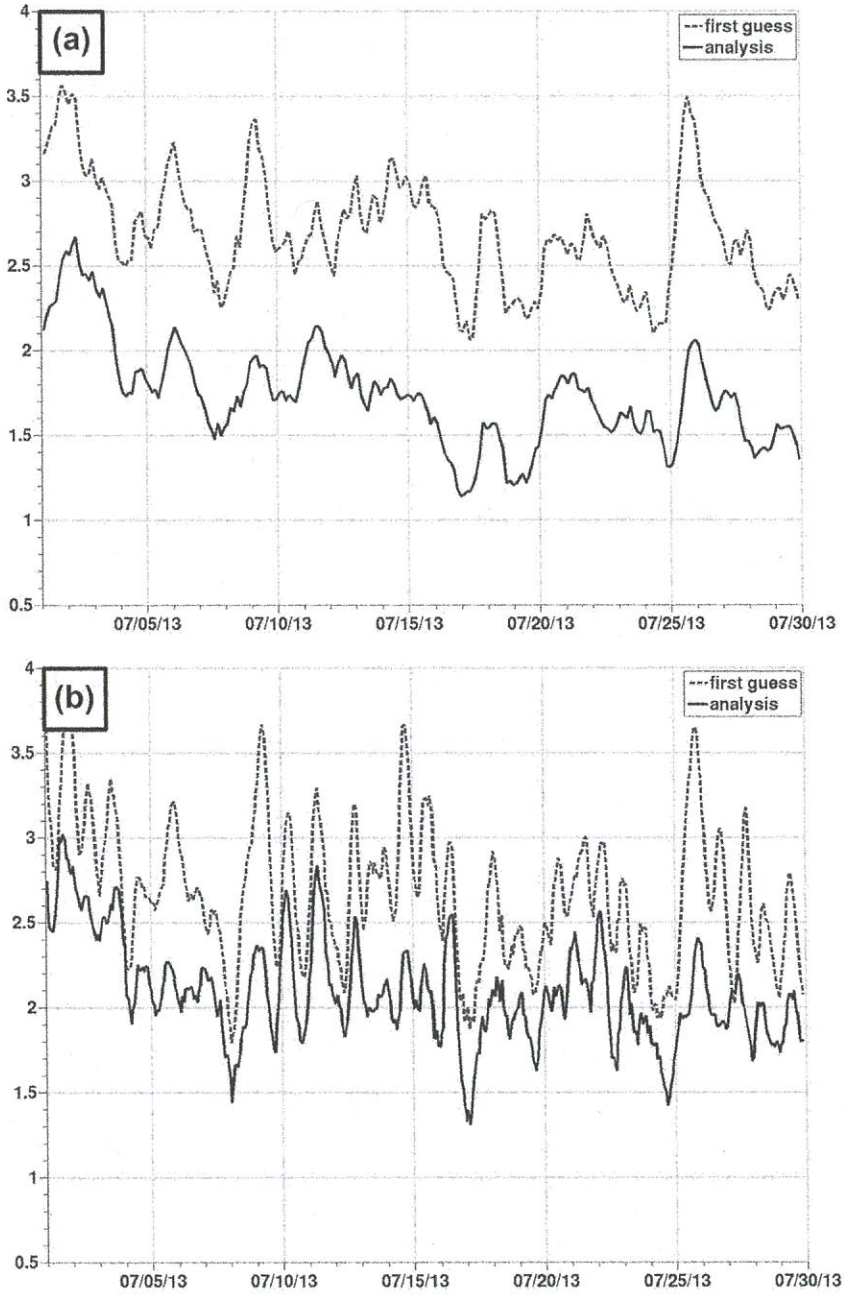


**FIGURE 3**

$J_{FIT}$ metric for the first guess solution (dashed) and the new assimilated solution (solid) at the assimilated observations every third hour (a) and at the withheld observations (b).

compared to assimilated observations, whereas Figure 3(b) shows similar $J_{FIT}$ values for the assimilated solution and the first guess compared to withheld observations. It can be seen that similar to the previous experiment, there is a significant reduction in the $J_{FIT}$ values from the first guess (2–3.5 standard deviations) to the assimilated solution (1.2–2.7 standard deviations). More importantly, there is a good improvement of the assimilated solution versus the first guess when these two solutions are compared to the withheld observations, an improvement that sometimes exceeds a standard deviation.

Figure 4 shows a comparison of surface velocities maps from the observations, the first guess, and the analysis 5 and 16 days into the assimilation, respectively. We first note that at these two time levels, there is almost no agreement at all between the circulation patterns shown in the observations and those in the first guess, i.e., the model is significantly in error compared to the observations, even after being initialized by the assimilation. For example, on day 5, the observations describe an offshore surface circulation, whereas the model shows an alongshore circulation. This results from the atmospheric forcing fields being erroneous themselves, see Figure 5. The assimilation procedure alters the first guess enough to produce an analysis that fits (looks like) the observations, albeit not perfectly: The offshore current is reconstructed by the assimilation on day 5; and on day 16, the northeastward coastal current that turns offshore is also recovered, though these features were missing in the first guess. However, the analysis sometimes still has the patterns of the first guess. This indicates that the background and model errors prescribed for the assimilation are too small.

A major difficulty in coastal ocean modeling resides in the lack of high spatial resolution atmospheric forcing. Atmospheric models are usually run with coarser resolutions compared to the ocean models (especially for coastal applications), because resolving the rather fast motion of the atmosphere with high horizontal resolution would require very small time steps that would be computationally prohibitive. For the case at hand, the ocean model has a horizontal resolution of 1 km, while the atmospheric forcing fields are obtained from interpolating results from an atmospheric model that used a 0.5° resolution that does not capture the variability of the model domain. According to Ekman theory, a modest wind stress of 5 m/s would cause the surface velocity to deflect to the right of the wind stress direction by an angle of 45° if the water depth is at least 45 m. The topography shown in Figure 1 indicates that this would not apply to a significant portion of the domain where the depth is less than 45 m, and it is expected that the surface velocity be strongly correlated to the wind stress in that part of the domain. Figure 5 shows the direction of the wind stress compared to the direction of the surface currents from the HF radar stations. The wind stress is generally uniform as a result of interpolating from a few grid points of the atmospheric model. It can be seen that the direction of the wind is never aligned with the direction of the observations; they are quite different. This presents a significant challenge to the assimilation system and explains why the assimilation could not accurately fit the observations with small initial conditions and model errors.

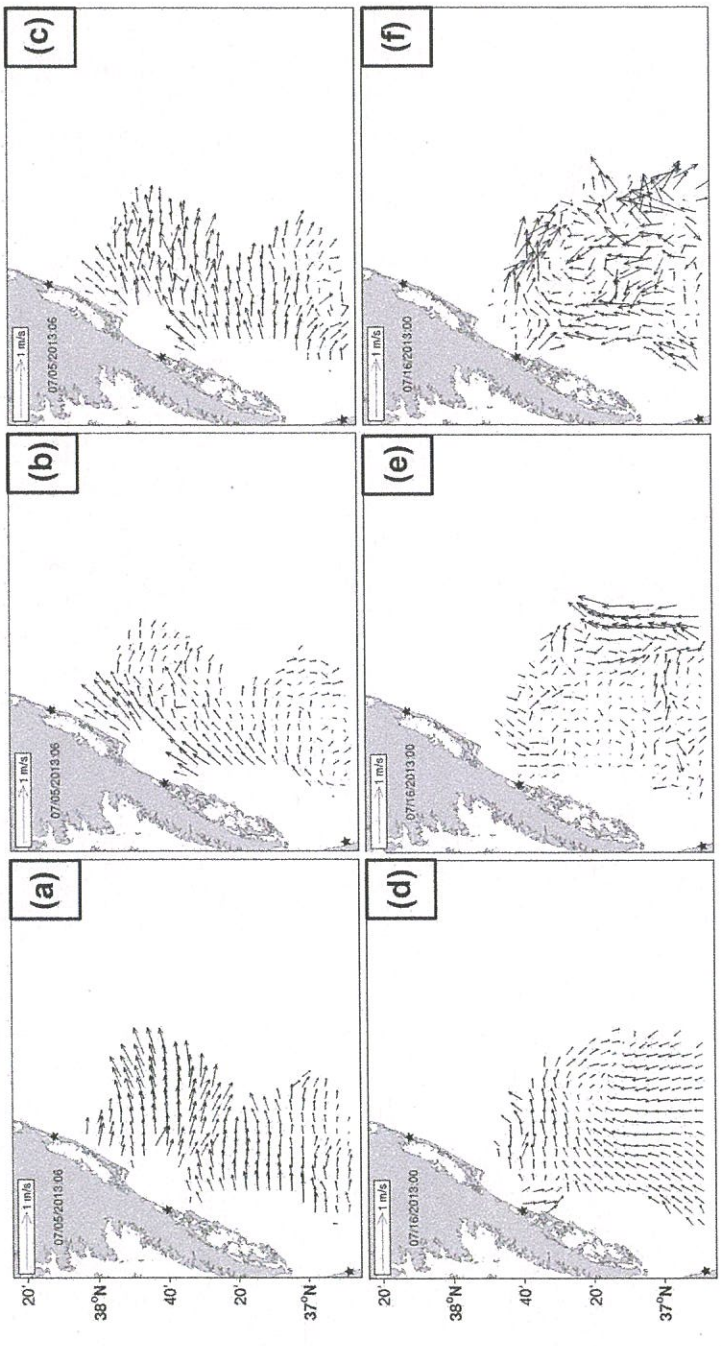


**FIGURE 4**

Surface velocities from the observations (a, d), the first guess (b, e), and the analysis (c, f) 5 and 16 days into the assimilation, respectively.

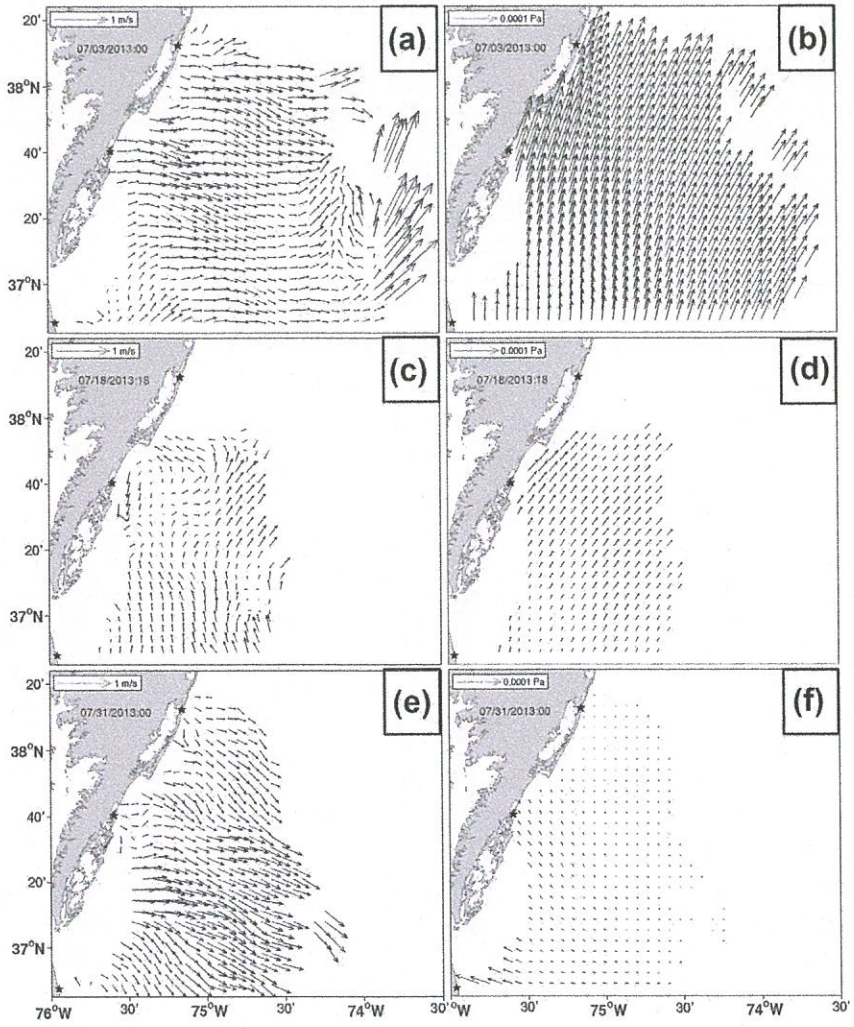


**FIGURE 5**

A comparison of the direction of the surface currents (a, c, and e) and the direction of the wind stress (b, d, and f) at the end of the first, the sixth, and the tenth assimilation window, respectively.

Another challenge to the assimilation resides in the resolution of the ocean model and that of the observations. The processed observations have a spatial resolution of about 6 km, whereas the model is run at a resolution of 1 km. As seen in Figure 6 in a subset of the domain, the model resolves multiple small-scale features that are absent from the observations. Also, the strong flow at the southeast corner of the domain reveals that the model boundary conditions contain an intrusion of the

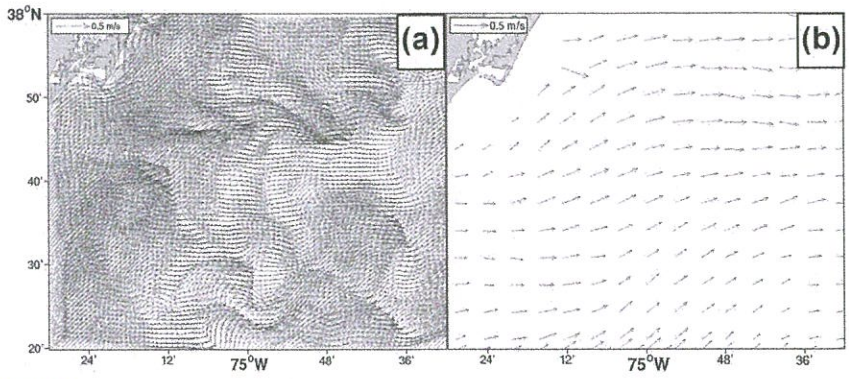


**FIGURE 6**

A comparison of the 1-km first guess velocity field (a) and the observations (b) on day 10 in a subset of the model domain.

Gulf Stream, another feature that is not present in the observations. Thus, the assimilation could benefit from more accurate boundary conditions and, perhaps, a slightly coarser resolution from the model, say 3 km.

A third assimilation experiment is carried out for three cycles of 3 days each, with the same setup as the original experiment, except that the model resolution is reduced from 1 to 3 km. Figure 7(a) shows a comparison between the analyses of the 1 and 3 km experiments, where significant improvements in the accuracy of the 3-km analysis can be seen, especially at the times when the 1-km analysis has $J_{FIT}$ values exceeding 1.5 standard deviations. In general, $J_{FIT}$ values for the 3-km analysis are lower than 1.5 standard deviations. On the other hand, a similar comparison of $J_{FIT}$ values for the first guesses from both 1- and 3-km experiments in Figure 7(b) shows that the forecast from the 3-km analysis has significantly improved compared to the 1-km forecast, with noticeable gaps between the two lines sometimes exceeding 1 standard deviation. However, the 3-km first guess still displays large discrepancies with the observation, having $J_{FIT}$ values generally exceeding 2 observation standard deviations, and only occasionally falling below 1.5 standard deviations. Once again, this loss of accuracy in the first guess is attributed to the erroneous atmospheric forcing (in this case the wind stress) because the model resolution is now closer to that of the observations coverage, and the analysis is also significantly closer to the observations.

Similar to Figure 4, Figure 8 shows a comparison of surface velocities maps from the observations, the first guess, and the analysis 3 and 5 days into the assimilation, respectively, for the 3-km model resolution. There is a significant difference in the direction of the velocity between the observations and the first guess on July 3, especially at the lower-right side of the domain showing an intrusion of the Gulf Stream in the first guess, whereas the observations locate this intrusion further to the east and slightly to the north, compared to its location in the first guess. The assimilation

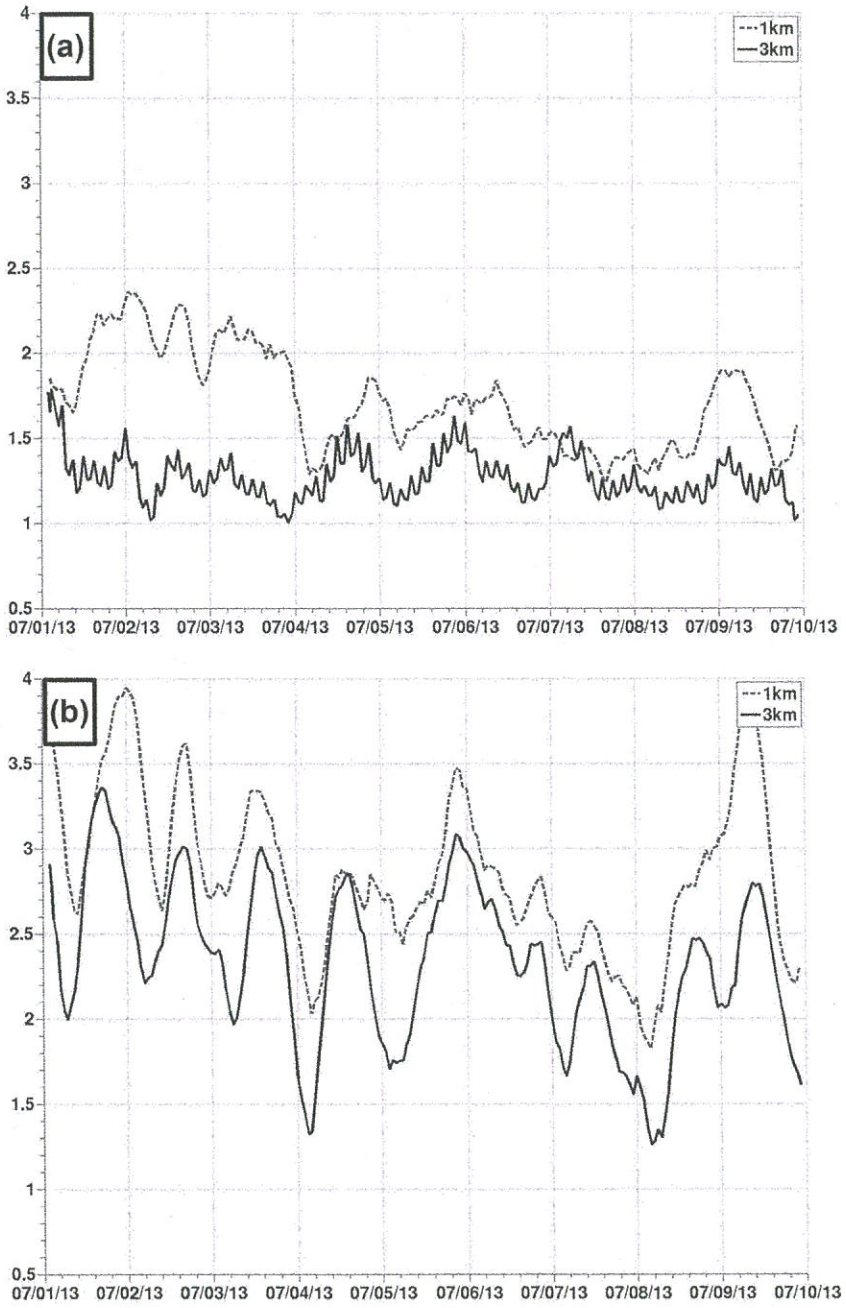


**FIGURE 7**

A comparison of the $J_{FIT}$ values from the analyses (a) and the first guesses (b) from the 1-km (dashed) and 3-km (solid) model resolutions.

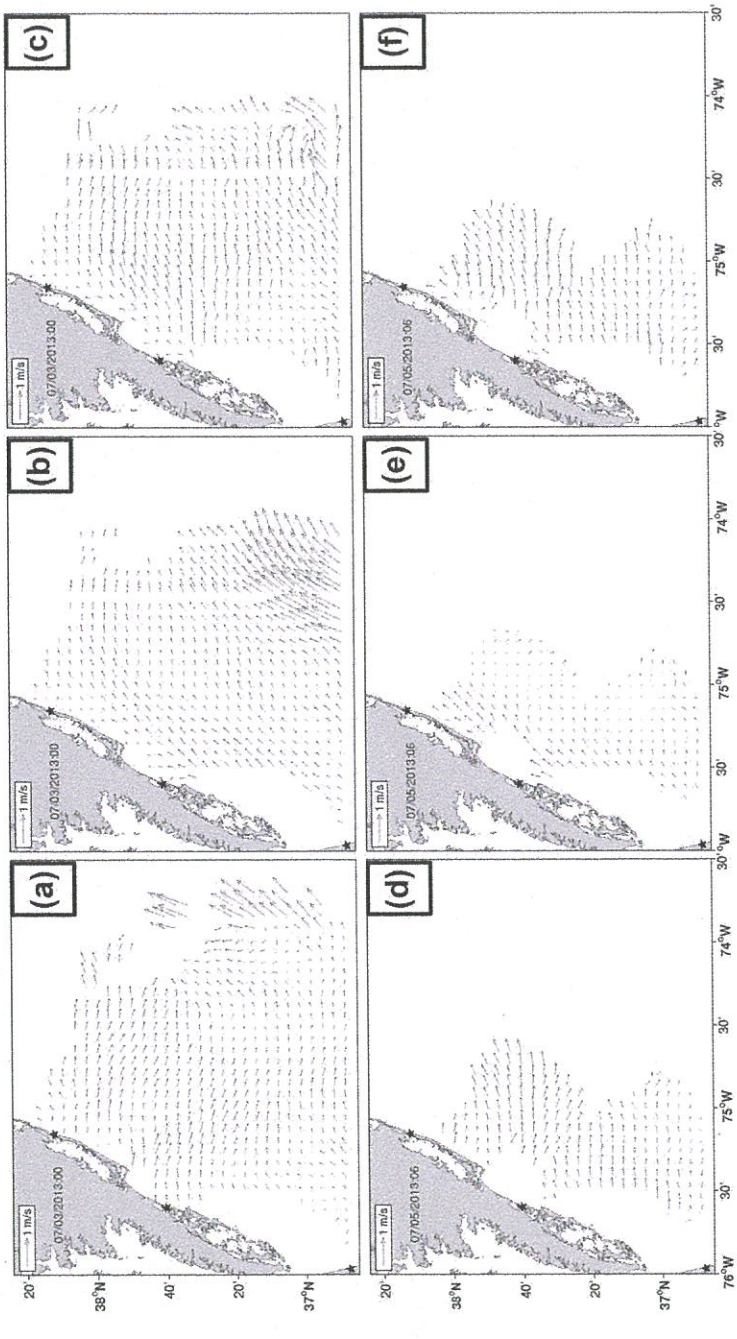


**FIGURE 8**

Similar to Figure 4, surface velocities from the observations (a, d), the first guess (b, e), and the analysis (c, f) on July 3 and July 5, respectively.

procedure corrects the first guess significantly to produce an analysis that fits (looks like) the observations, e.g., the Gulf Stream current is in better agreement with the observations, albeit not perfectly. However, the analysis on July 3 still has some patterns of the first guess, indicating that the background and model errors prescribed for the assimilation may still be too small. The analysis on July 5 shows a much better agreement with the observations (offshore circulation), even though the first guess was not (coastal circulation). Thus, even in the presence of an erroneous wind stress, the weak constraint assimilation fits the observations significantly better when the model's horizontal resolution is closer to that of the observations coverage.

## 7. CONCLUSION

Surface velocity observations from HF radar are a valuable data set for monitoring the coastal circulation, and they can be assimilated into a coastal circulation ocean model using the NCOM-4DVAR system, provided adequate model resolution, initialization, boundary conditions, and atmospheric forcing. It was shown in the experiments presented here that the assimilation cannot accurately fit the observations with rather small initial conditions and model errors. However, the biggest challenge for the assimilation system consists in an erroneous wind stress that consistently steers the model in a completely different direction than the observed surface velocities. Although the assimilation was able to reduce a noticeable portion of the model's discrepancy to the observations, those gains were quickly lost in the forecast stage for the following assimilation window, primarily due to the wrong wind stress and the high resolution of the model. Reducing the model resolution to be closer to that of the observations significantly improved the accuracy of the analysis and the forecast. The ability of the assimilation system to accurately fit the observations can also be improved by prescribing higher model errors. However, we suggest that instead of increasing the error levels in the assimilation system, which can be justified for the case at hand, the primary source of the errors must be addressed first, i.e., providing a wind stress that drives the model to be in more agreement with the observations. This can be achieved by a local nest of the atmospheric model, or better yet, a fully coupled ocean–atmosphere model.

## ACKNOWLEDGMENTS

This work was sponsored by the Office of Naval Research Program Element 0601153N as part of "A multiscale Approach for Assessing Predictability of ASW environment" and "Rapid Transition NCOM-4DVAR" projects. The authors would like to thank the two anonymous reviewers whose constructive comments helped to improve the quality of this paper. The authors would also like to acknowledge Teresa Updyke at the Center for Coastal Physical Oceanography at Old Dominion University for freely providing the HF radar data used in this study and Rich Pawlowicz for providing the freely available M_MAP Matlab toolbox used here. This paper is NRL contribution number NRL/BC/7320-14-1231-4004.

## REFERENCES


1. Oke PR, Allen JS, Miller RN, Egbert GD, Kosro PM. Assimilation of surface velocity data into a primitive equation coastal ocean model. *J Geophys Res* 2002;**107**:3122. http://dx.doi.org/10.1029/2000JC000511.
2. Paduan JD, Shulman I. HF radar data assimilation in the Monterey Bay area. *J Geophys Res* 2004;**109**:C07S09. http://dx.doi.org/10.1029/2003JC001949.
3. Barth A, Alvera-Azcárate A, Weisberg RH. Assimilation of high-frequency radar currents in a nested model of the West Florida Shelf. *J Geophys Res* 2008;**113**:C08033.
4. Li Z. A multi-scale three-dimensional variational data assimilation scheme and its application to coastal oceans. In: *Proceedings of the 9th workshop on adjoint model applications in dynamic meteorology, Cefalu, Sicily, Italy*; 2011. http://gmao.gsfc.nasa.gov/events/adjoint_workshop-9/presentations/Li.pdf.
5. Hoteit I, Cornuelle B, Kim SY, Forget G, Köhl A, Terrill E. Assessing 4D-VAR for dynamical mapping of coastal high-frequency radar in San Diego. *Dyn Atmos Oceans* 2009;**48**:175–97.
6. Zhang WG, Wilkin JL, Arango HG. Towards an integrated observation and modeling system in the New York Bight using variational methods. Part I: 4DVAR data assimilation. *Ocean Modell* 2010;**35**(3):119–33.
7. Yu P, Kurapov A, Egbert GD, Allen JS, Kosro PM. Variational assimilation of HF radar surface currents in a coastal ocean model off Oregon. *Ocean Modell* 2012;**49–50**: 86–104. http://dx.doi.org/10.1016/j.ocemod.2012.03.001.
8. Ngodock HE, Carrier MJ. A 4D-Var assimilation system for the Navy coastal ocean model part I: system description and assimilation of synthetic observations in the Monterey Bay. *Mon Weather Rev* 2014:2085–107. http://dx.doi.org/10.1175/MWR-D-13-00221.1.
9. Carrier MJ, Ngodock HE, Smith SC, Jacobs GA, Muscarella PA, Ozgokmen T, et al. Impact of assimilating ocean velocity observations inferred from Lagrangian drifter data using the NCOM-4dvar. *Mon Weather Rev* 2014;**142**(4):1509–24.
10. Roarty H, Glenn S, Kohut J, Gong D, Handel E, Rivera E, et al. Operation and application of a regional high-frequency radar network in the Mid-Atlantic Bight. *Mar Technol Soc J* 2010;**55**(6).
11. Lipa BJ, Barrick DE. Least-squares methods for the extraction of surface currents from CODAR cross-loop data: application at ARSLOE. *IEEE J Oceanic Eng* 1983;**OE-8**: 226–53. http://dx.doi.org/10.1109/JOE.1983.1145578.
12. Paduan JD, Rosenfeld LK. Remotely sensed surface currents in Monterry Bay from shore-based HF radar (coastal ocean dynamics application radar). *J Geophys Res* 1996;**101**:20669–86.
13. Martin P. *Description of the navy coastal ocean model version 1.0*. 2000. NRL report NRL/FR/7322—00-9961.
14. Barron CN, Kara AB, Martin PJ, Rhodes RC, Smedstad LF. Formulation, implementation and examination of vertical coordinate choices in the global navy coastal ocean model (NCOM). *Ocean Modell* 2006;**11**:347–75.
15. Goerss JS, Phoebus PA. The Navy's operational atmospheric analysis. *Weather Forecast* 1992;**7**:232–49.
16. Rosmond TE. The design and testing of the navy operational global atmospheric prediction system. *Weather Forecast* 1992;**7**:262–72.

17. Rosmond TE, Teixeria J, Peng M, Hogan TF, Pauley R. Navy operational global prediction system (NOGAPS): forcing for ocean models. *Oceanography* 2002;**15**:99–106. http://dx.doi.org/10.5670/oceanog.2002.40.
18. Bennett AF. *Inverse methods in physical oceanography*. New York: Cambridge University Press; 1992. 347 pp.
19. Bennett AF. *Inverse modeling of the ocean and atmosphere*. Cambridge University Press; 2002.
20. Ngodock HE, Chua BS, Bennett AF. Generalized inversion of a reduced gravity primitive equation ocean model and tropical atmosphere ocean data. *Mon Weather Rev* 2000;**128**: 1757–77.
21. Ngodock HE, Carrier MJ. A weak constraint 4D-Var assimilation system for the navy coastal ocean model using the representer method. In: Park SK, Xu L, editors. *Data assimilation for atmospheric, oceanic and hydrologic applications*, vol. II. Springer-Verlag Berlin Heidelberg; 2013. http://dx.doi.org/10.1007/978-3-642-35088-7_15.